



Flow imaging using differential Golay encoded ultrasound

A. Nowicki, J. Tasinkiewicz^{*}, I. Trots

Ultrasound Department, Institute of Fundamental Technological Researches of the Polish Academy of Sciences, Warsaw, Poland

ARTICLE INFO

Keywords:

Coded excitation
Flow imaging
Ultrasound imaging
Classical beamforming

ABSTRACT

In our research we present a new method of differential compression of the Golay encoded ultrasound (DCGEU) in the standard beamforming mode to visualize the slow ($<1\text{cm/s}$) blood mimicking fluid flow in small diameter tubes. The proposed DCGEU method is based on synthesis of several subsequent B-mode frames acquired with certain time intervals (30 ms in this study) followed by the visualization of differential beamformed radio frequency (RF) echoes, which yielded the images of the scatterers moving slowly in the vessel and suppressing the static echoes outside the vessel. In order to extract small backscattered echoes from the vessel area we took an advantage of improved sensitivity of the complementary Golay coded sequences (CGCS).

The validation of the proposed DCGEU method was carried out in two stages. In the first one, we compared the flow images in small tubes with a diameter of 1 mm and 2.5 mm, reconstructed from numerically simulated acoustic data for the standard transmission of short pulses and 16-bits long CGCS signals. In the second stage of the research, the experimental data were acquired in a flow phantom with silicone tubes with an internal diameter of 1.5 mm and 4.5 mm and a fluid flow velocity of 0.9 cm/s. The experiments were carried out using preprogrammed Verasonics Vantage™ research ultrasound system equipped with ALT L12-5/50 mm MHz linear array transducer with 7.8 MHz center frequency.

It was evidenced both in simulations and experiments that the DCGEU provided a good flow image along the entire length of tubing with virtually angle independent detection in comparison with the conventional short pulse interrogation.

1. Introduction

In recent years, there have been reports and apparatus enabling very sensitive flow imaging, especially in Doppler Power (PD) modality using new adaptive clutter filters and noise bias elimination. The selection of the high pass frequency limit is a key element of the slow flow visualization with pulsed wave PD. At 8 MHz setting the high pass filter to 50 Hz corresponds to cutting off flows below 0.5 cm/s. Often, the displacement of tissue (breathing) and the movements of the operator's hand generate frequencies close to those resulting from blood flow, masking the tested perfusion of the organs under study [1,2]. New effective methods of clutter filtration include adaptive demodulation-based high pass filter techniques [2] or by using the spatio-temporal characteristic of the Doppler acquired echoes. Demene et al. [3] demonstrated that singular value decomposition of ultrafast acquisition of ultrasonic data allows to separate space and time filters (blood/tissue discrimination) from the Casorati matrix [4]. Nayak et al. [5] proposed normalized cross-correlation (NCC)-based speckle tracking technique to

estimate tissue displacements and allowing for motion correction prior to singular value decomposition of echoes ensemble data. Their approach considerably improved clutter rejection, emphasizing the flow images in small vessels. This method is to some extent a modification of clutter filter correction for tissue movements in contrast agent imaging of small vessels [6,7]. Bayet et al. [8] proposed a two-step algorithm to enhance vessel-background separation directly on the power Doppler images by exploiting blood echo-noise independence. The above-mentioned methods of correction of clutter filtration require advanced computational techniques.

The main objective of our research was to propose a new, simple and intuitive approach to the technique of emphasizing small signals from small vessels against the background of large tissue signals. The method is based on imaging of differential sequences of beamformed radio frequency (RF) echoes from the complementary Golay coded sequences (CGSC) transmission. Specifically, the aim of our study was to demonstrate that DCGEU imaging of fluid flow using two consecutive CGCS significantly improves the slow flow imaging in small diameter tubes

^{*} Corresponding author.

E-mail address: yurijtas@ippt.pan.pl (J. Tasinkiewicz).

<https://doi.org/10.1016/j.ultras.2022.106825>

Received 12 November 2021; Received in revised form 23 May 2022; Accepted 11 August 2022

Available online 17 August 2022

0041-624X/© 2022 Elsevier B.V. All rights reserved.

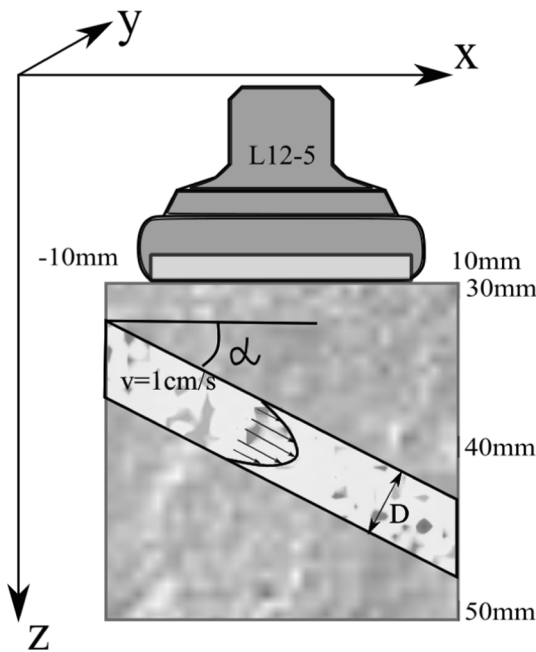


Fig. 1. Field II simulation of the data flow in the tube of diameter D inclined at the angle α with respect to the transducer face. The 1 cm/s flow of parabolic profile was simulated.

compared to the standard short pulse interrogation.

The paper is organized as follows. In the next Section the details of numerical simulation in Field II and experimental measurements set-up are discussed. Also the brief theoretical fundamentals of the Golay encoded transmission are outlined. In the Section 3 the results of numerical simulations and experimental measurements are presented. Discussion and conclusions of the obtained results are presented in the Sections 4 and 5, respectively.

2. Methods

We tested the proposed DCGEU approach using numerical acoustic data simulated in Field II [9] program for Matlab® for 1 mm and 2.5 mm tubes and flow velocity of 1 cm/s. Moreover, we conducted in vitro measurements in a flow phantom with silicone tubing with inner diameters of 1.5 mm and 4.5 mm and slow (0.9 cm/s) blood mimicking

fluid (CIRS model 046 blood mimicking fluid, CIRS Tissue Simulation Technology, Norfolk, VA) driven by gravity using Verasonics Vantage™ research ultrasound system equipped with ALT L12-5/50 mm MHz linear array transducer with 7.8 MHz center frequency. In simulations and measurement set-up the tubes were inclined at 5° and 10° with respect to the transducer face.

2.1. Field II simulations

In the first step of our research, we validated the proposed DCGEU flow imaging method using numerically simulated acoustic data. For this purpose, a 128-element 7.8 MHz linear array transducer was modeled in Matlab® using Field II simulation software. The pitch was 0.195 mm and the element width was 0.17 mm. These two parameters were chosen to imitate the L12-5/50 mm array transducer used in the vitro experiments (see discussion in the next section). Two types of transmitted signal were used: a short pulse (one cycle burst at the transducer nominal frequency) and the 16 bits long CGCS sequences with one cycle at the center carrier frequency per bit. The flow data were simulated in tubes of different diameters D (1 mm and 2.5 mm) with wall of infinitesimal thickness. The flow direction was set at two angles of 5° and 10° with respect to the transducer face (Fig. 1).

The flow of 0.9 cm/s with parabolic profile was simulated. The tube was placed in the scattering medium modeled by random uniform distribution of point-like scatterers in the volume of $z \times x \times y = 20 \text{ mm} \times 20 \text{ mm} \times 5 \text{ mm}$. In order to approximate Rayleigh scattering, the number of point scatterers was chosen to be $\sim 30 \text{ per mm}^3$, which results in $60 \cdot 10^3$ point-like scatterers in the volume under consideration.

The ratio of backscattered amplitude from a scatterer within the tube area (fluid) to the backscattered amplitude from a scatterer outside the tube area (surrounding tissue) was 1/10. The ultrasound data acquisition is explained below (see Fig. 2).

In transmit (TX) mode 32 adjacent elements (sub-aperture) were activated to generate acoustic field for given excitation signal (short pulse or CGCS pair). Next, the same sub-aperture was switched to the receive (RX) mode and each element recorded back-scattered signal independently. For the CGCS excitation two subsequent transmissions were required (code A and code B, see Fig. 4) to obtain a single compressed radio-frequency (RF) echo. The CGCS signal compression is discussed in Section 2.3.

After completing the data acquisition all 32 recorded (and compressed in the case of CGCS pair) RF echoes were synthesized into a single beamformed scan-line. Specifically, the scan-line along the sub-

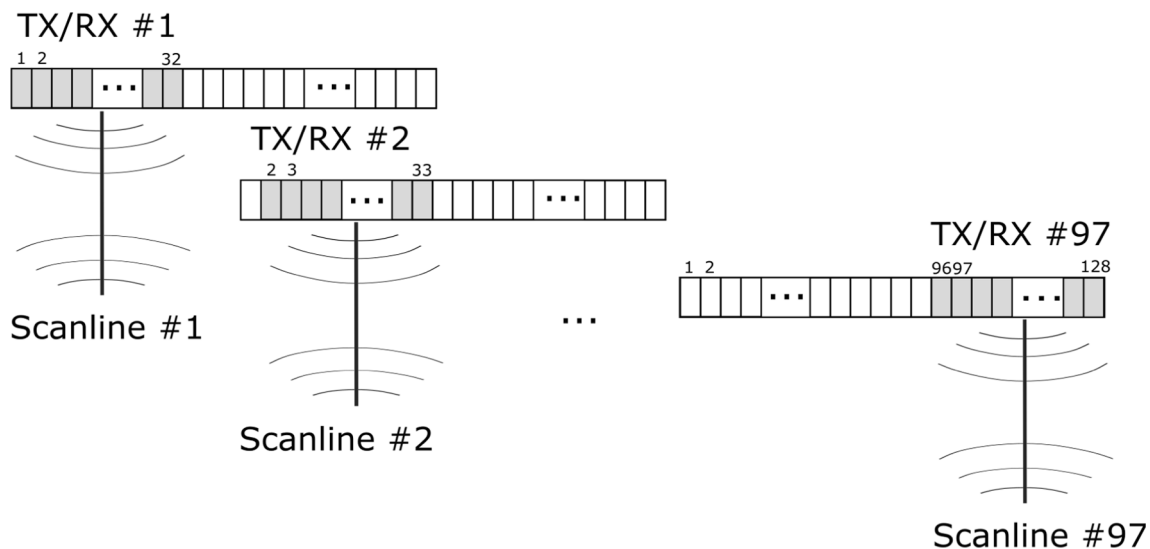


Fig. 2. Acoustic data acquisition diagram in classical beam forming mode using 32 elements in TX/RX mode and one element stride between scan lines.

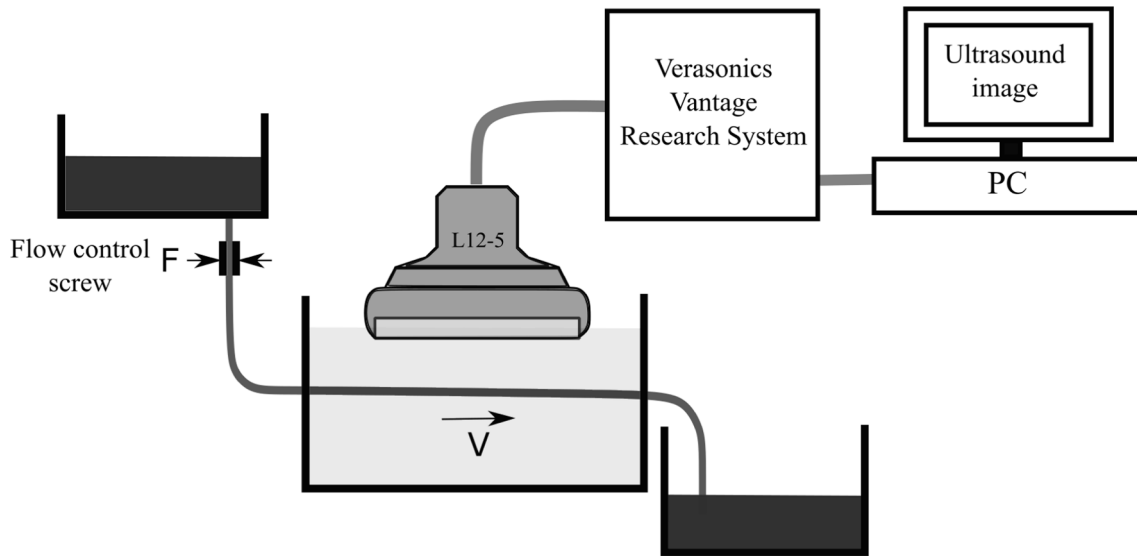


Fig. 3. Schematic diagram of the flow imaging experimental set-up.

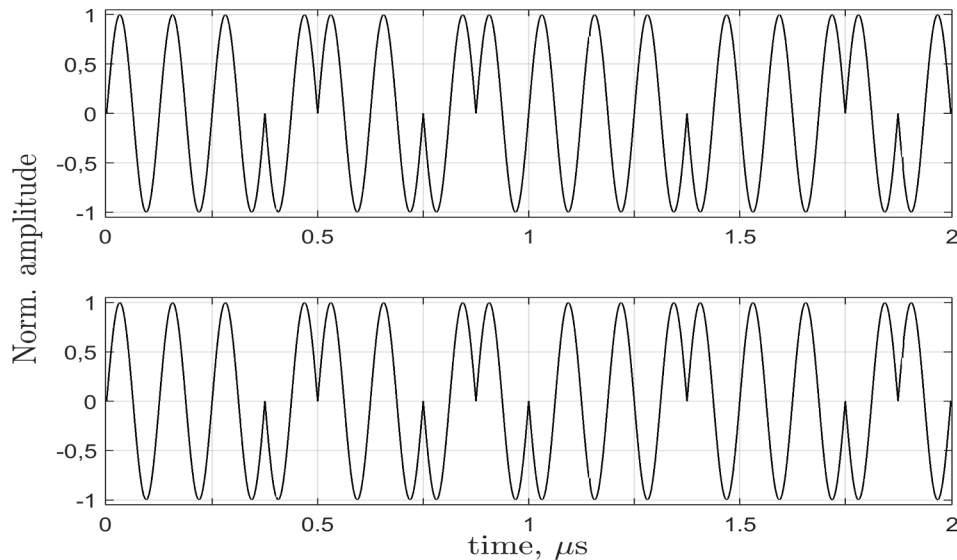


Fig. 4. 16-bit CGCS pair of encoded signals used in numerical simulations and experimental measurements. Top panel – the code A and the bottom panel – the code B. Each bit of the code represented by a single sine cycle.

aperture axis was synthesized based on the delay-and-sum (DAS) beamforming including dynamic focusing in RX mode. In a similar way ultrasound data for all 97 scan-lines were acquired (data acquisition cycle) each time shifting the TX/RX sub-aperture by one element along the transducer and repeating the ultrasound data acquisition for a new TX/RX sub-aperture setting. A single data acquisition cycle yielded ultrasound data required for a single B-mode image comprised of 97 scan-lines.

The DCGEU flow imaging method presented in this paper requires only 2B-mode images to be reconstructed. The time period T of the subsequent acoustic data acquisition cycles was set to 30 ms (which corresponded to the frame rate of 33 Hz). During 30 ms the scatterers in the tube displaced by approximately 0.3 mm for a given flow velocity of 0.9 cm/s.

In order to simulate the real flow measurements conditions the white Gaussian noise was added to the simulated backscattered echoes. For this purpose, we first estimated the standard deviation σ_s of the simulated backscattered signal of arbitrary chosen RF line alone. Specifically,

the line #64 in the TX/RX sub-aperture #48 which corresponded to the scan-line #48 in the middle of the synthesized B-mode image was chosen. To estimate the standard deviation of the back-scattered signal σ_s the time-gated part of the echo from the tube area was used. Next, we generated the white Gaussian noise with two different values of standard deviation $\sigma_n = (0.1; 0.5)\sigma_s$ and added them to each of the simulated RF echoes (the time-trace of the white noise was different for each RF echo simulated by the Field II).

Having the subsequent B-mode image frames synthesized, the difference of their RF scan-lines (or, alternatively, the difference of the corresponding envelopes obtained using the Hilbert transform) results in the differential flow imaging. Specifically, 97 scan-lines were synthesized using DAS beamforming of the RF echoes $S_{RF}(t)$ recorded in each step of the data acquisition cycle (Fig. 2) yielding a single RF image frame. Applying the Hilbert transform to each of the 97 synthesized RF scan-lines and calculating the echoes magnitude $S_E(t)$ along each scan-line we finally obtained a single B-mode image frame. After time T , the ultrasound data acquisition cycle was repeated and the next frames

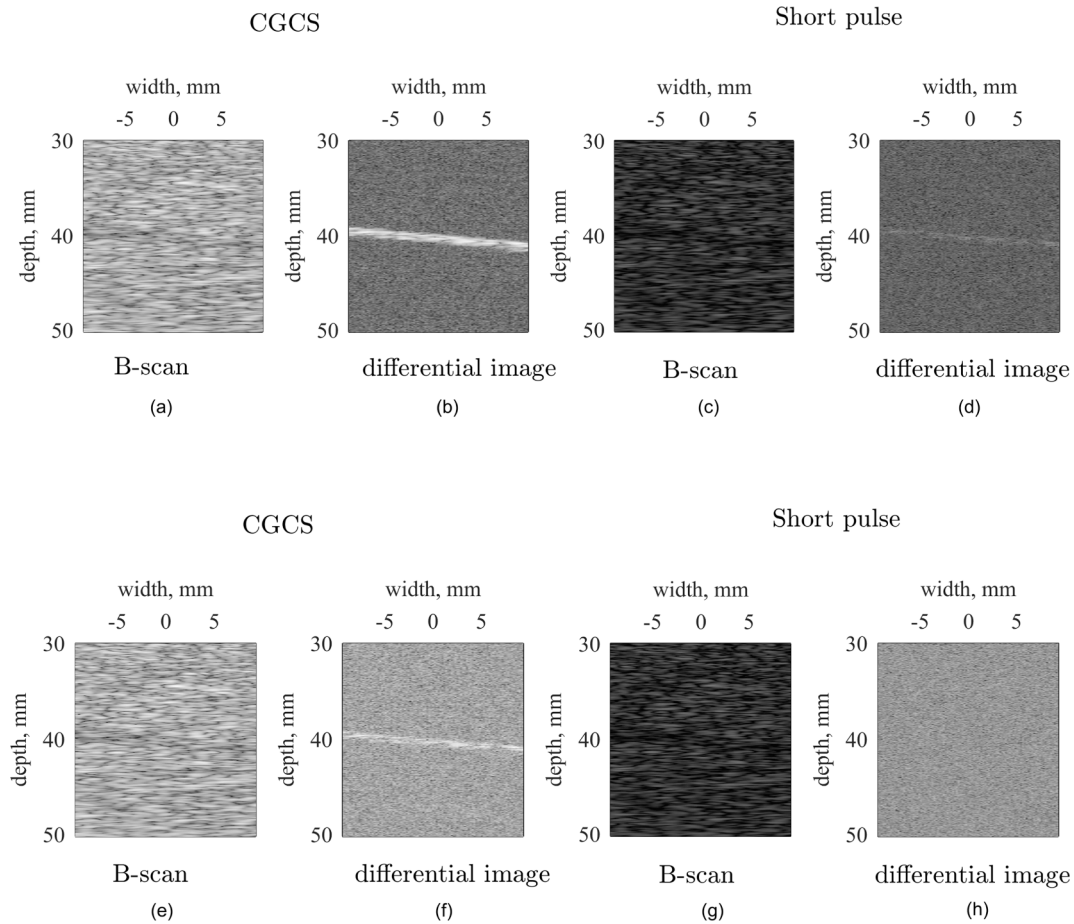


Fig. 5. B-mode and differential images of the numerically simulated flow data in 1 mm tube for 5° inclination with respect to the transducer face. The white Gaussian noise with standard deviation (a) – (d) $\sigma_n = 0.1\sigma_s$ and (e) – (h) $\sigma_n = 0.5\sigma_s$ was added to simulated echoes.

were synthesized, $S_{RF}(t+T)$ and $S_E(t+T)$, and so on, yielding $S_{RF}(t+NT)$ and $S_E(t+NT)$ for $N+1$ image frames reconstructed.

The basic idea of the DCGEU method presented in this study was to find the difference of the RF image frames followed by the envelope detection (envelopes obtained using the Hilbert transform applied to RF difference) to visualize only the scatterers in the tube area that had been displaced during time nT and eliminate the stationary echoes from the surrounding tissue elements. In this study the differential images were computed using Eq. (1):

$$\Delta S_{RF}(nT) = HT\{S_{RF}(t+(i+n)T) - S_{RF}(t+iT)\}, i = 0 \dots N, n = 1, N-1. \quad (1)$$

where HT denotes the Hilbert transform, computed using the ‘*hilbert.m*’ routine from the *Signal Processing Toolbox* in Matlab®.

Alternatively, the difference between successive signal envelopes (B-mode images) is given by:

$$\Delta S_E(nT) = S_E(t+(i+n)T) - S_E(t+iT), i = 0 \dots N, n = 1, N-1, \quad (2)$$

where $S_E(t) = HT\{S_{RF}(t)\}$.

2.2. Experimental measurements

The proposed method was verified using experimentally obtained flow data. The experimental setup is shown schematically in Fig. 3. The flow of the blood mimicking fluid was forced gravitationally and the flow velocity was adjusted manually by flow control screw. It allowed obtaining the flow velocity of 0.9 cm/s in tubes with internal diameters of 1.5 mm and 4.5 mm and wall thickness of 1.5 mm and 0.45 mm,

respectively.

The ultrasound data for the flow phantom were acquired using the Verasonics Vantage™ Research System (Kirkland, WA) equipped with the L12-5 linear array transducer operating at 7.8 MHz center frequency. The excitation voltage was 9.8 V with 8 dB amplification of the received signals. The scanner was preprogrammed to scan the phantom according to the data acquisition scheme described in the Section 2.1 (see Fig. 2) using 32 TX/RX sub-aperture and one element stride between transmissions in a single data acquisition cycle needed to synthesized 97 scanlines comprising a single B-mode image. In our experiments the backscattered echoes were acquired in 6 subsequent frames. Two types of transmitted signal were programmed: the short pulse and the 16 bits long CGCS with one cycle of the center carrier frequency per bit (similar excitations was used also in Field II simulations). In the later case two successive transmissions of the code A and code B in each TX/RX sub-aperture position were programmed to obtain a single compressed RF echo. The period of subsequent data acquisition cycles (between B-mode frames) was 30 ms as in the Field II numerical simulations. The amplitude of the transmitted signal for the CGCS and the short pulse was the same, which corresponded to the excitation voltage of 9.8 V.

To estimate the efficiency of coded transmission in the DCGEU imaging method the *signal-to-noise ratio* (SNR), defined as the ratio of the average signal power to the RMS noise power [10] was assessed and compared for the CGCS and short pulse transmissions. It was determined from the beamformed RF signals along the scan line #48 of the differential B-mode images of the 4.5 mm at different inclinations with respect to the transducer face. The average signal power was determined using time gated echoes in the tubing area. Specifically, the 3.5 mm (about 18 wavelengths) window, centered with respect to the tube axis was used

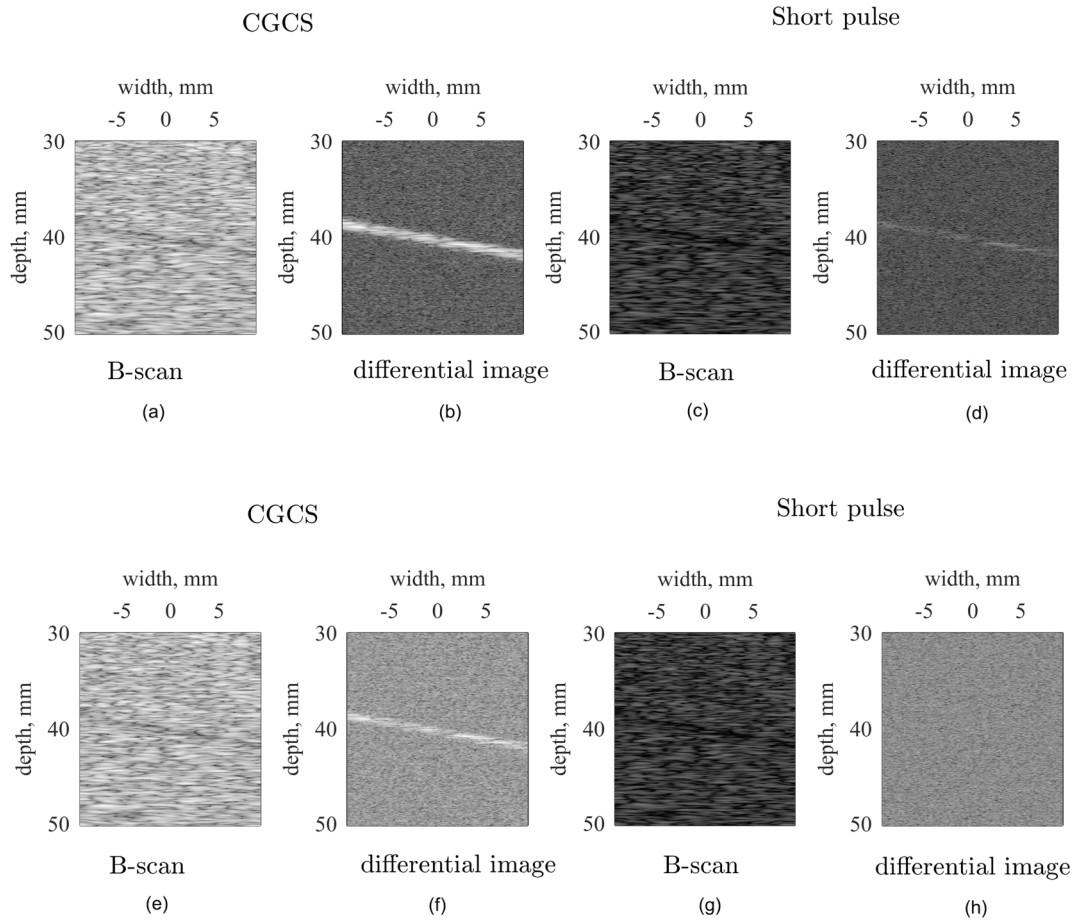


Fig. 6. B-mode and differential images of the numerically simulated flow data in 1 mm tube for 10° inclination with respect to the transducer face. The white Gaussian noise with standard deviation (a) – (d) $\sigma_n = 0.1\sigma_s$ and (e) – (h) $\sigma_n = 0.5\sigma_s$ was added to simulated echoes.

for the signal power assessment. The RMS noise power was estimated over the time gated beamformed signal within the 10 mm window (about 50 wavelengths) starting from 35 mm to 45 mm depth, assuming at that depth only the noise was present in the recorded signal. Prior the SNR computing, the sample rate of the beamformed RF signals was increased by a factor of 16 in Matlab® using *interp.m* routine.

Also, the contrast-to-noise ratio (CNR), introduced by Patterson and Foster [11] and the generalized CNR (gCNR) introduced by Rodrigues-Morales et al in [12] were estimated for the differential images of the flow data acquired with the CGCS and the short pulse excitation signals. Specifically, the CNR was defined as follows:

$$CNR = \frac{|\mu_B - \mu_T|}{\sqrt{\sigma_B^2 + \sigma_T^2}}, \quad (3)$$

where μ_T and μ_B are the mean signal power inside the tube and noise in the background region, respectively, whereas σ_T and σ_B are the corresponding variances of signal power inside the tube and in noise in the background region.

According to [12] the definition of gCNR is as follows:

$$gCNR = C^{-\frac{c}{c-1}} - C^{-\frac{1}{c-1}}, \quad C = \frac{\mu_B}{\mu_T}. \quad (4)$$

The mean signal power μ_T and the variances of signal power σ_T inside the tube were estimated over the region in the form of a parallelogram R_T with its sides parallel to the tube walls and centered with respect to its axis of symmetry, as depicted in the Fig. 11 (f) in Section 3.2. The mean noise power μ_B and the variance of noise power were estimated over the region R_B of the same shape as the R_T region and placed in a distance of 1.5 mm below the tube (see Fig. 11 (f)).

For the 4.5 mm tubing the axial dimension of the R_T and R_B regions (the length of the vertical sides of the parallelogram aligned along the z -axis direction) was 3.5 mm, whereas the lateral dimension, defined as a distance between the vertical sides of the was 5 mm.

Moreover, the efficiency of echoes amplitude gain was estimated recording reflected signals from a brass plate immersed in distilled and degassed water. Both, the short pulse and CGCS pairs were programmed as transmit signals.

2.3. CGCS signal processing

The Golay codes belong to a wider class of complementary algebraic codes [13]. Complementary Golay coded sequences (CGCS) consist of a pair of codes of length N , whose autocorrelation functions have side lobes of the same value but opposite signs. As a result, the sum of the autocorrelation functions yields the single peak of amplitude $2N$ for its argument equal to zero and vanishes otherwise [14]. The 16 bits long CGCS used in our research has a form:

$$A_{16} = \{1, 1, 1, -1, 1, 1, -1, 1, 1, 1, -1, -1, -1, 1, -1\};$$

$$B_{16} = \{1, 1, 1, -1, 1, 1, -1, 1, -1, -1, -1, 1, 1, 1, -1, 1\},$$

and is shown graphically in Fig. 4.

The process of transmitting-receiving and compressing the CGCS pair is briefly outlined below:

- (1) Transmit the A code (the first of the pair CGCS, Fig. 4, top panel).
- (2) Receive the echoes for the code A.

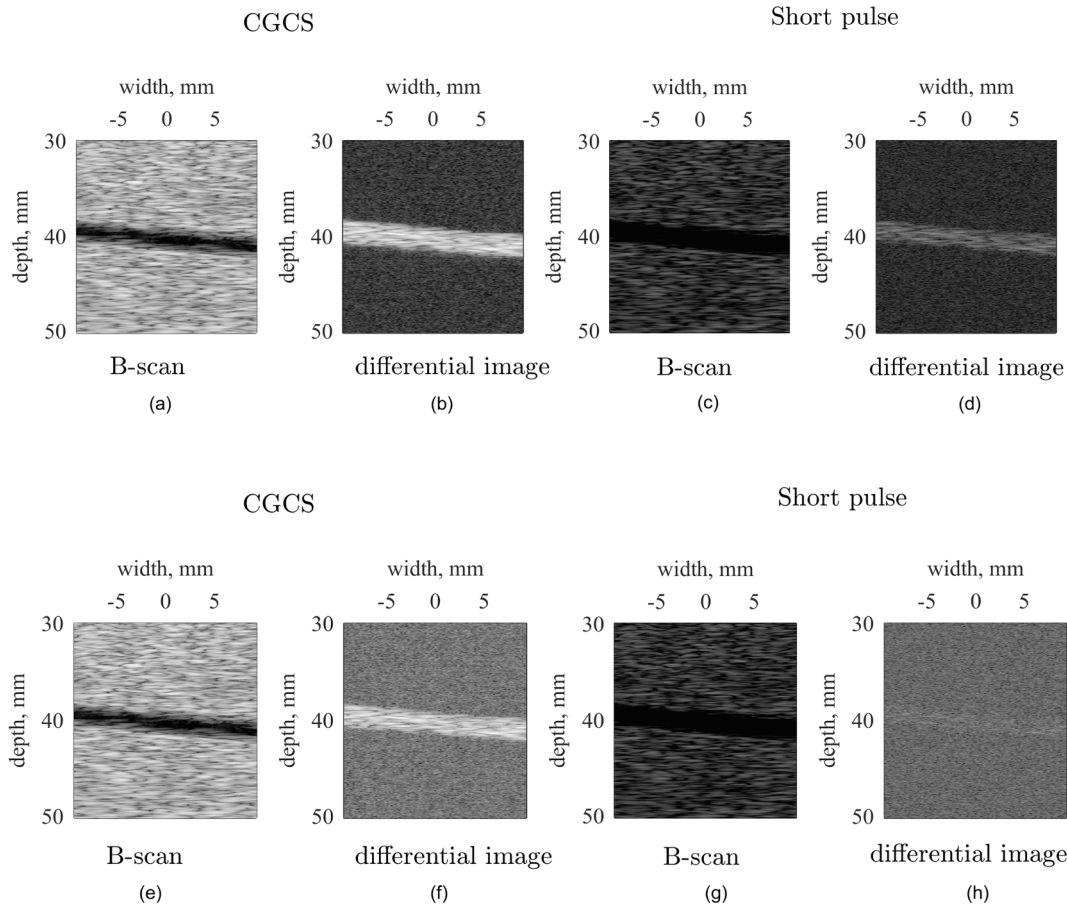


Fig. 7. B-mode and differential images of the numerically simulated flow data in 2.5 mm tube for 5° inclination with respect to the transducer face. The white Gaussian noise with standard deviation (a) – (d) $\sigma_n = 0.1\sigma_s$ and (e) – (h) $\sigma_n = 0.5\sigma_s$ was added to simulated echoes.

- (3) Transmit the B code (the second of the pair of CGCS, Fig. 4, bottom panel).
- (4) Receive the echoes for the code B.
- (5) Compute the correlation functions of codes A and B with corresponding echoes.
- (6) Compute the compressed RF echo by summation of the correlation functions obtain in the step 5.

It should be noted that double transmission is associated with a twofold extension of the signal acquisition time and a double time compression. Moreover, any movement of the object between successive transmissions causes the appearance of side lobes resulting from decorrelation between echoes.

3. Results

3.1. Field II simulations

The B-mode images of the numerically simulated flow data in the tubes of 1 mm and 2.5 mm in diameter and flow direction angle of 5° and 10° are shown in Figs. 5–8 for different excitation signals - the 16-bit long CGCS pair and the short pulse and different white Gaussian noise level. Namely, both the B-modes of a single frame and differential imaging of the flow data acquired with the CGCS excitation and the short pulse are shown. The B-modes of a single frame (denoted as ‘B-scan’ in the Figs. 5–8 and also in Figs. 10–12 in the Section 3.2) were reconstructed using classical beamforming mode discussed in the Section 2.1. In turn, the differential images were obtained taking the difference of the synthesized (beamformed) RFs in two subsequent B-mode frames for

specified excitation signal. All images (i.e. the envelopes of the beamformed RF signals corresponding to the image) were normalized with respect to the maximum value in the CGCS and short pulse excitations sets of the beamformed RF signals prior visualization. In the Field II simulations the B-mode images and the differential images are displayed over 50 dB and 60 dB dynamic ranges, respectively.

3.2. Measurements

First, the efficiency of echoes amplitude gain was estimated recording echoes from perfect reflector immersed in distilled and degassed water. Fig. 9 shows the short pulse echo from the perfect reflector (Fig. 9(a)) and the compressed CGCS echo recorded with the linear array L12-5 transducer (Fig. 9(b)). The amplitude gain was approximately 7.6 (17.6 dB).

Next, the differential flow imaging with CGCS transmission was compared with the short pulse excitation using experimental flow data in the 1.5 mm and 4.5 mm tubes inclined by 5° and 10° with respect to the transducer face. The flow velocity for recorded cases was equal to 0.9 cm/s (adjusted with the flow control screw, see Fig. 3). The results, both the B-modes of a single frame and differential imaging of the flow data acquired with the CGCS excitation and the short pulse are shown in Figs. 10 and 11. All B-mode images and the differential images below are displayed over 50 dB dynamic range.

The assessed values of the SNR, CNR and gCNR (see Section 2.2) obtained for the 4.5 mm tubing and different flow direction with respect to transducer face are presented in Table 1.

To confirm that the area of the tube filled with non-moving fluid did not stand out from the surrounding media in the differential image for

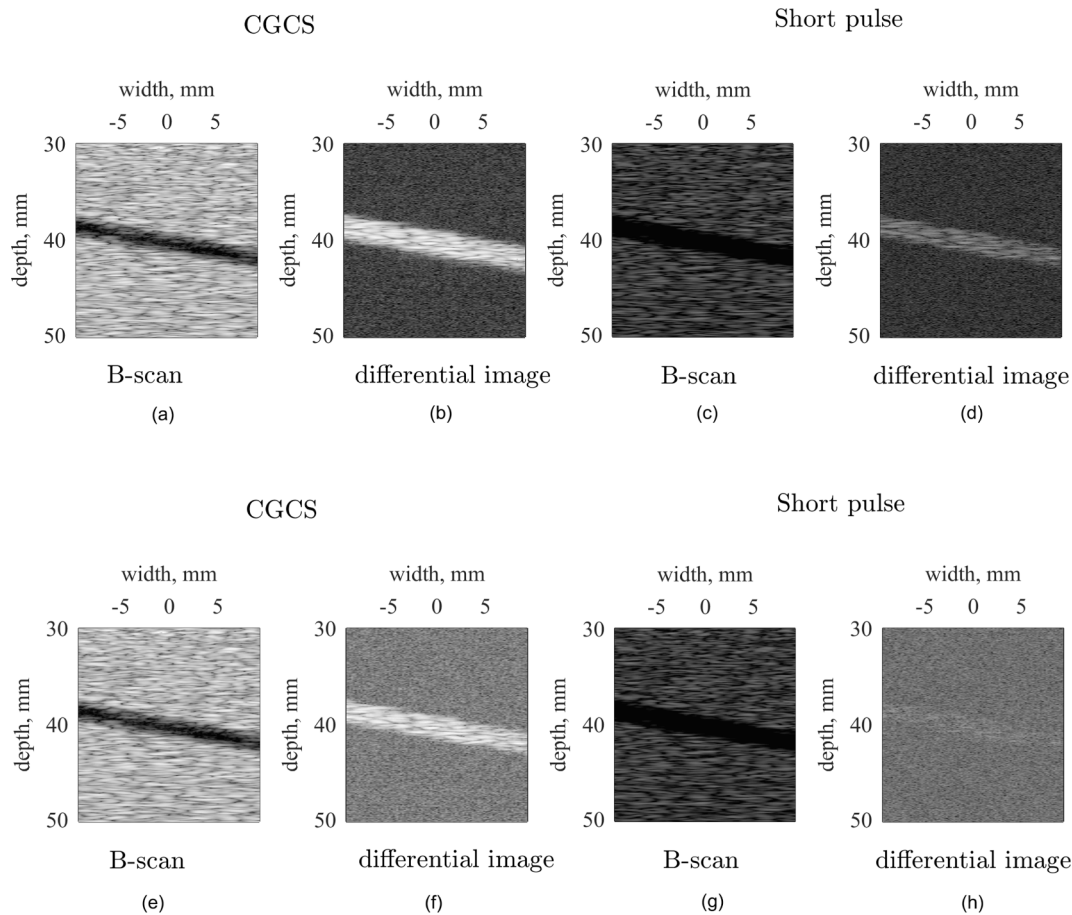


Fig. 8. B-mode and differential images of the numerically simulated flow data in 2.5 mm tube for 10° inclination with respect to the transducer face. The white Gaussian noise with standard deviation (a) – (d) $\sigma_n = 0.1\sigma_s$ and (e) – (h) $\sigma_n = 0.5\sigma_s$ was added to simulated echoes.

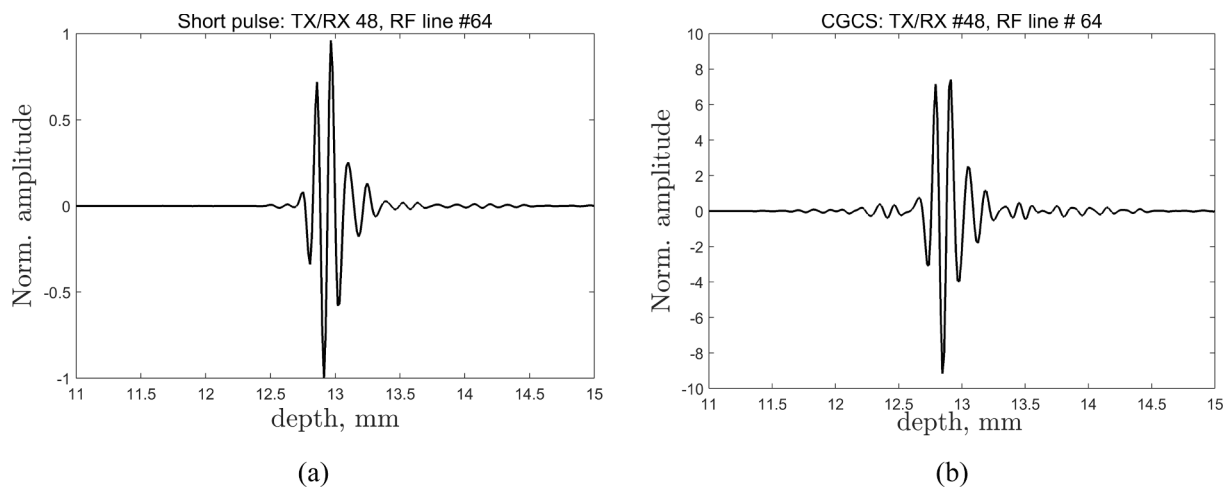


Fig. 9. Echoes from the perfect reflector immersed in distilled and degassed water; left signal recording - short pulse transmission and right signal recording - for 16 bits CGCS pair. The amplitude gain is 7.6.

the CGCS and short pulse transmissions, another experiment was conducted in which the flow in the tube was stopped. As we can see in Fig. 12(b) and (d), the differential images in the tube area do not differ in gray-scale from the images outside the tube. This confirms that the actually proposed DCGEU method enables detection of the backscattering particles movements even at low speeds, filtering out from the final image the backscattered echoes from the stationary targets.

4. Discussion

The results presented in this paper confirmed feasibility of the slow blood flow imaging in small vessels by the proposed DCGEU method. Also, the effectiveness of the CGCS transmission over conventional short pulse interrogating signal was demonstrated both in the Field II simulations and in-vivo measurements. In Figs. 10 and 11 we can clearly observe that in the center of the tube, the echo is practically not visible

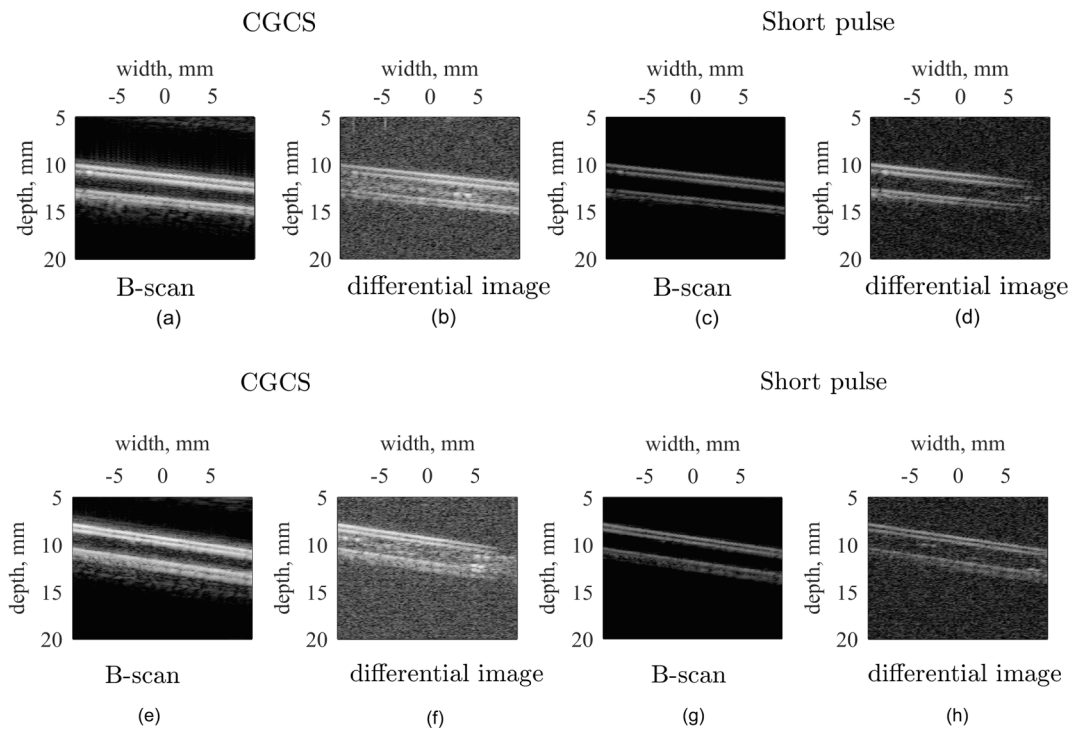


Fig. 10. B-mode and differential images of experimental flow data acquired from the 1.5 mm tube for (a) – (d) 5° and (e) – (h) 10° inclinations with respect to the transducer face.

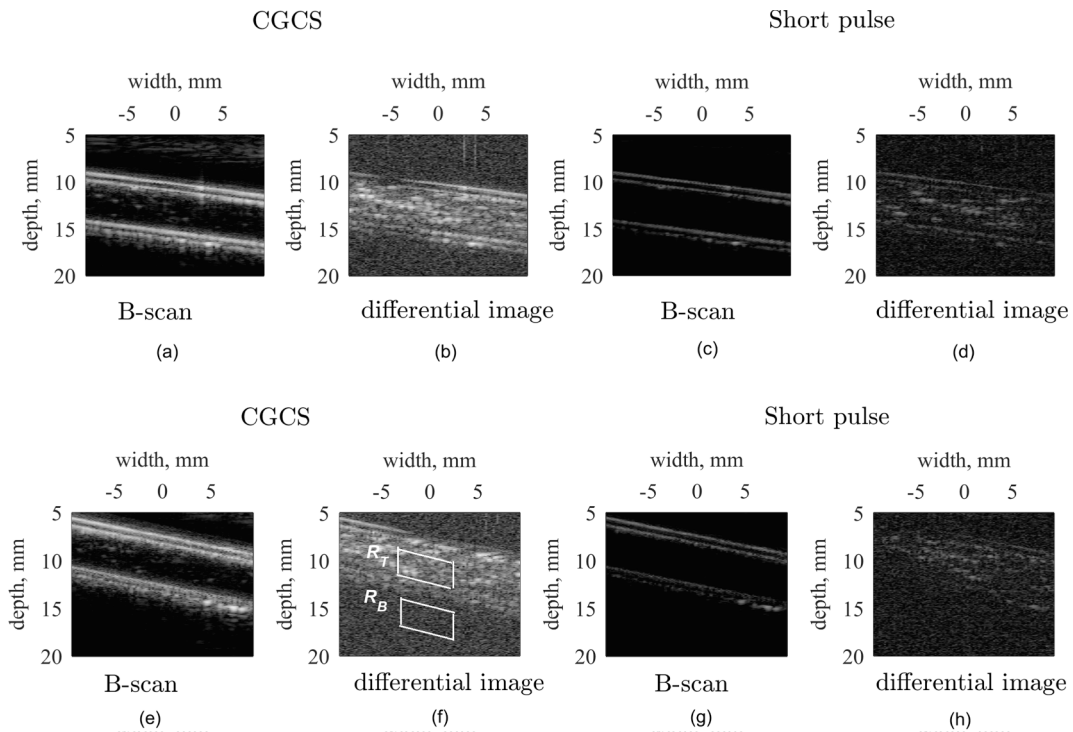


Fig. 11. B-mode and differential images of experimental flow data acquired from the 4.5 mm tube for (a) – (d) 5° and (e) – (h) 10° inclinations with respect to the transducer face. In Fig. 11 (f) the regions R_T and R_B are shown (see Section 2.3) which were used to compute the CNR and gCNR parameters referred in Table 1.

in the B-mode images, while in the differential images obtained with the transmitted CGCS signal the flow (change in position of the scatterers in the tube) was clearly recorded. This observation is also clearly manifested in simulations presented in Figs. 5–8.

Due to the CGCS transmission the DCGEU method yielded about

17.6 dB gain in amplitude of the compressed echoes in comparison to the short pulse interrogation signal, as shown in Fig. 9. This, in turns, resulted in the SNR increase for the beamformed RF echoes in the vessel. Specifically, the estimated SNR values for 4.5 mm tube confirmed increase in the SNR not less than 8 dB for the CGCS excitation in

Table 1
SNR, CMR and gCNR for CGCS and pulse transmission for 4.5 mm tubing and different flow directions.

Parameter	CGCS		Short pulse	
	5°	10°	5°	10°
SNR	14.9 dB	12.9 dB	5.6 dB	4.8 dB
CNR	0.65	0.51	0.43	0.41
gCNR	0.89	0.82	0.49	0.48

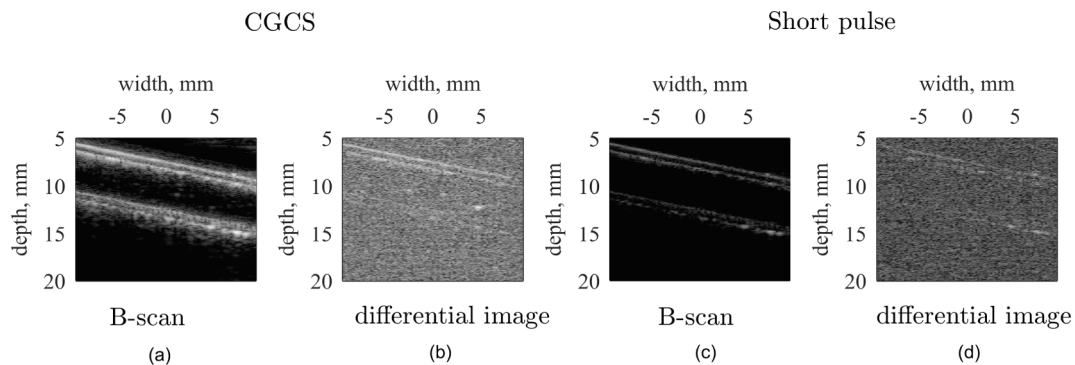


Fig. 12. B-mode and differential images of experimental flow data acquired from the 4.5 mm tube filled with blood-mimicking fluid without flow and 10° inclinations with respect to the transducer face.

comparison to the short pulse signal in the case of flow direction of 5°. The corresponding increase in SNR of approximately 9.3 dB was observed for 10° inclination angle of the tubing with respect to the transducer face. The difference in the estimated SNR increase might have been caused by slight change in the head positioning. Similarly, significant increase in the gCNR parameter was observed. Specifically, due to the CGCS transmission the gCNR increased from 0.49 to 0.89 for 5° inclination angle and from 0.48 to 0.82 for 10° flow direction in comparison to the short pulse transmission.

The limited frequency bandwidth of the applied L12-5 linear array transducer resulted in important distortion of coded echoes and as previously reported in [15] to significant reduction in amplitude gain after the echo compression. The bandwidth of the applied linear array transducer was less than 60 % theoretically resulting in over 50 % gain reduction of the final compressed echo. It might explain that in our experiments, the amplitude gain of the signal reflected from the perfect reflector (Fig. 9) was only 7.6 (17.6 dB) comparing to the theoretical gain of 32 (30 dB) for the signal compression using transducer-receiver channel with 100 % bandwidth. One could expect much better differential flow images for a transducer-receiver channel system with considerably elevated bandwidth.

Numerical simulations and experimental measurements confirmed that good quality of B-mode flow images along the entire length of the tube with practically angle-independent detection can be obtained by CGCS transmission in the DCGEU method compared to the conventional short pulse transmission.

In the images presented in Figs. 10–12 we can see incompletely filtered echoes from the walls of the tubes. Theoretically, a complete echo reduction from a stationary target was to be expected. Unfortunately, the rather high noise level of the receiving channel causes differences in the instantaneous amplitude of large echoes in successive image frames. In addition, large echoes are burdened with non-linear distortions, which means that, along with the noise, their difference from subsequent image frames after compression does not completely cancel out. However, this is not a significant drawback of the system. Residual stationary echoes do not reduce the clear flow images from moving scatterers.

In our future work, we will try to overcome the limitation related to the bandwidth of the transducer and receiver by doubling the bit length

in a 16-bit CGCS, i.e. two cycles of the transducer operating frequency per bit of the code will be transmitted. This approach is expected to reduce the bandwidth related distortion in the received echoes, improving the compression efficiency and consequently reducing the amplitude of the side lobes, as it was reported in [16].

We will try to optimize the code length for the use of the in vivo system in the imaging of small vessels in neoplastic lesions of the thyroid gland and breast.

5. Conclusions

In this work we presented the differential compression of Golay encoded ultrasound imaging method DCGEU. We demonstrated the feasibility of slow blood flow imaging in small vessels with the DCGEU. The method takes advantage of the Golay coded transmission to improve the SNR of small backscattered echoes detected from moving scatterers distributed within the vessel.

This, in turns, enables visualization of differential echoes in the vessel and suppresses the stationary echoes outside the vessel. The DCGEU method was verified using flow data obtained by numerical simulation in Field II and experimentally recorded data. The results of comparative study confirmed significant improvement in discrimination of the fluid flow in the tube area for the CGCS transmission in comparison to the conventional short pulse transmission.

Declaration of Competing Interest

The authors declare that they have no known competing financial interests or personal relationships that could have appeared to influence the work reported in this paper.

References

- [1] A.C.H. Yu, L. Lovstakken, Eigen-based clutter filter design for ultrasound color flow imaging: A review, *IEEE Trans. Ultrason. Ferroelectr. Freq. Control* 57 (5) (2010) 204–216.
- [2] J. Tierney, C. Coolbaugh, T. Towse, B. Byram, Adaptive clutter demodulation for non-contrast ultrasound perfusion imaging, *IEEE Trans. Med. Imaging* 36 (9) (2017) 1979–1991.

- [3] C. Deme ne, et al., Spatiotemporal clutter filtering of ultrafast ultrasound data highly increases Doppler and fultrasound sensitivity, *IEEE Trans. Med. Imaging* 34 (2015) 2271–2285.
- [4] E.J. Candes, C.A. Sing-Long, J.D. Trzasko, Unbiased risk estimates for singular value thresholding and spectral estimators, *IEEE Trans. Signal Process.* 61 (19) (2013) 4643–4657.
- [5] R. Nayak, M. Fatemi, A. Alizad, Adaptive background noise bias suppression in contrast-free ultrasound microvascular imaging, *Phys. Med. Biol.* 64 (2019), 245015.
- [6] J. Foiret, H. Zhang, T. Ilovitsh, L. Mahakian, S. Tam, K.W. Ferrara, Ultrasound localization microscopy to image and assess microvasculature in a rat kidney, *Sci. Rep.* 7 (1) (2017) 13662.
- [7] V. Hingot, C. Errico, M. Tanter, O. Couture, Subwavelength motion-correction for ultrafast ultrasound localization microscopy, *Ultrasonics* 77 (2017) 17–21.
- [8] M. Bayat, M. Fatemi, A. Alizad, Background removal and vessel filtering of noncontrast ultrasound images of microvasculature, *IEEE Trans. Biomed. Eng.* 66 (3) (2019) 831–842.
- [9] J.A. Jensen, Field: A Program for Simulating Ultrasound Systems, in: 10th Nordic-Baltic Conference on Biomedical Imaging Published in Medical & Biological Engineering & Computing, 34, Supplement 1, Part 1, 351–353, 1996.
- [10] T. Misaridis, Ultrasound imaging using coded signals, Center for fast ultrasound imaging technical university of Denmark, Phd Thesis, 2009.
- [11] M.S. Patterson, F.S. Foster, The improvement and quantitative assessment of b-mode images produced by an annular array/cone hybrid, *Ultrasonic Imaging* 5 (3) (1983) 195–213.
- [12] A. Rodriguez-Molares, O.M.H. Rindal, J. D’hooge, S.-E. Masoy, A. Austeng, M. A. Lediju Bell, H. Torp, The generalized contrast-to-noise ratio: A formal definition for lesion detectability, *IEEE Trans. Ultrason. Ferroelectr. Freq. Control.* 67 (4) (2020) 745–759.
- [13] M. Golay, Complementary series, *IRE Trans. Inf. Theory* 7 (2) (1961) 82–87.
- [14] I. Trots, A. Nowicki, W. Secomski, J. Litniewski, Golay sequences - sidelobe-cancelling codes for ultrasonography, *Arch. Acoust.* 29 (1) (2004) 87–97.
- [15] A. Nowicki, I. Trots, P.A. Lewin, W. Secomski, R. Tymkiewicz, Influence of the ultrasound transducer bandwidth on selection of the complementary Golay bit code length, *Ultrasonics* 47 (1–4) (2007) 64–73.
- [16] I. Trots, A. Nowicki, M. Postema, „Ultrasound image improvement by code bit elongation, *IEEE Signal Process. Lett.* 25 (3) (2018) 437–441.